KERNFORSCHUNGSANLAGE JÜLICH GmbH

Institut für Plasmaphysik
Association EURATOM-KFA

SPECTROSCOPIC STUDY OF ATOMIC BEAMS GENERATED BY LASER ABLATION OF MULTI-LAYER TARGETS

by

R. Koppmann, S.M. Refaei, A. Pospieszczyk

Jül - 1986
March 1985
ISSN 0366-0885

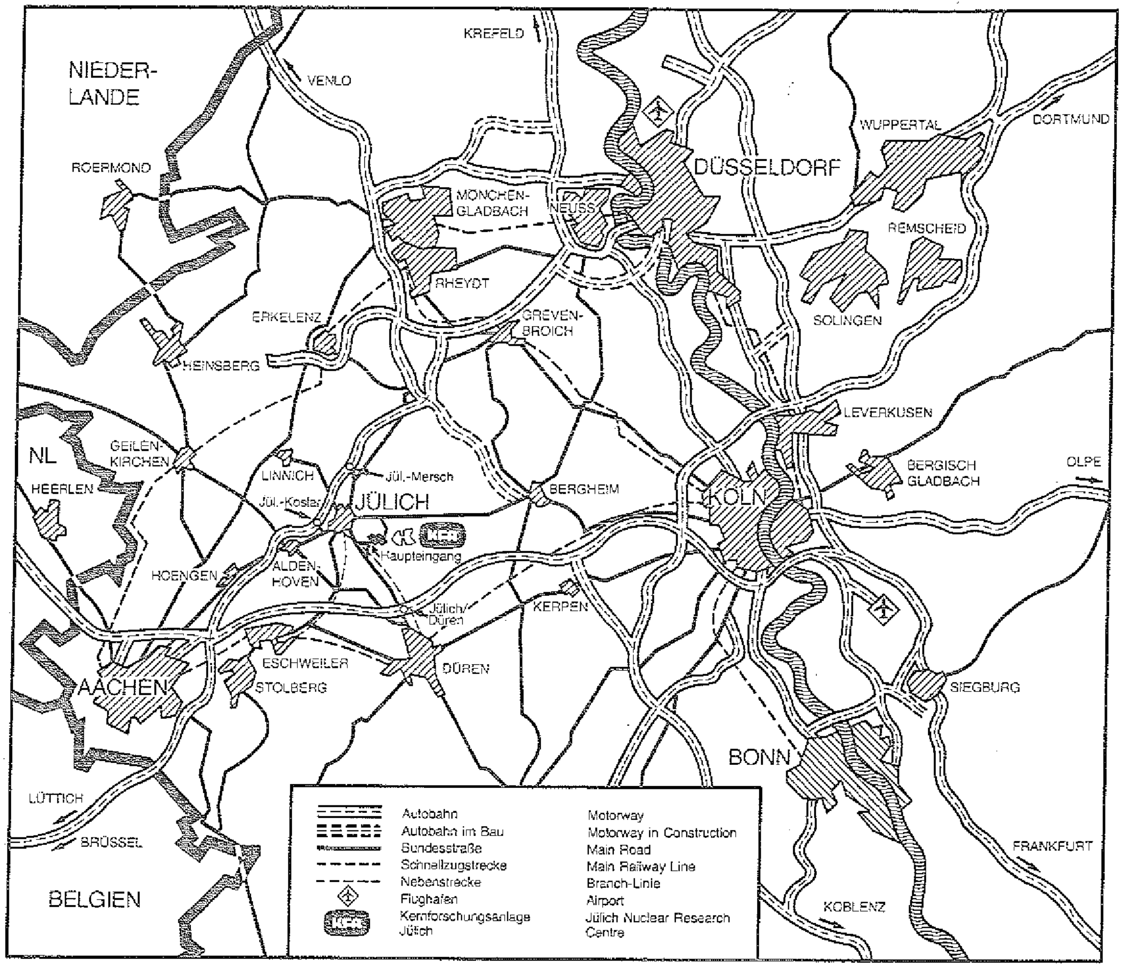

Als Manuskript gedruckt

Berichte der Kernforschungsanlage Jülich – Nr. 1986

Institut für Plasmaphysik, Association EURATOM-KFA Jül - 1986

Zu beziehen durch: ZENTRALBIBLIOTHEK der Kernforschungsanlage Jülich GmbH
Postfach 1913 · D-5170 Jülich (Bundesrepublik Deutschland)
Telefon: 02461/610 · Telex: 833556-0 kf d

SPECTROSCOPIC STUDY OF ATOMIC BEAMS GENERATED BY LASER ABLATION OF MULTI-LAYER TARGETS

by

R. Koppmann, S.M. Refaei, A. Pospieszczyk

Spectroscopic Study Of Atomic Beams Generated By Laser Ablation of Multi-Layer Targets.

R. Koppmann, S.M. Refaei*, A. Pospieszczyk.

Institut für Plasmaphysik der Kernforschungsanlage Jülich GmbH

Association EURATOM-KFA, 5170 Jülich, FRG.

Abstract

An experiment is described where Li- and Al-beams were generated by ablation of thin, multi-layer targets using a Q-Switched ruby laser with a total energy density up to 30 Jcm^{-2}. Measurements using laser induced fluorescence and mass spectroscopy were combined to analyse the energy- and density distribution and the temporal structure of the beams. The maximum energy turned out to be several eV for Li and several 10 eV for Al with a peak density in the range of 10^{10} cm^{-3} for both Li and Al.

The targets were analysed by optical microscopy and secondary ion mass spectroscopy providing information about the size of the spots and the structure of the metal film before and after the ablation experiment.

* present address: Cairo University, Faculty of Science, Physics Department, Cairo, Egypt.

1. Introduction

High power laser irradiation of a metal-film glass interface has been frequently used to generate intense, short bursts of high intensity energetic atom beams. The injection of such beams into a plasma at preselected times allows

- to study the effects of impurity ions on hydrogen plasmas
- to measure impurity transport processes independent of impurity ions naturally present in the plasma
- to determine the plasma boundary parameters using the neutral atom beams as a diagnostic tool /1,2,3/

For the injection of metal impurities the laser blow-off technique has been used successfully to produce 10^{16} - 10^{18} particles with energies of several 10 eV. A pulsed high power Q-switched solid state laser is normally used to ablate metal coated glass slides with a coating thickness up to 10 µm from the rear side. Several laboratory experiments have studied the properties of beams produced with this technique /3,4,5,6/.

The following experiment was carried out to determine the characteristics of the various atomic components emitted from irradiated multi-layer targets.

2. Experimental

The experimental set-up consists of

- a Q-switched ruby laser with a total energy of 0.5 J and pulse duration of 20 nsec,
- an HV-chamber and a drift tube with a base pressure of 10^{-6} mbar,
- a target, which can be manipulated from outside without breaking the vacuum
- several diagnostic systems.

The ruby laser beam was focussed into the vacuum system by two lenses of 133 cm and 6 cm local length, respectively. During all measurements the laser beam was diverted by a double periscope prism system and hit the target from the rear side through the glass. The periscope system can be moved up and down to allow also shots from the front of the target. in this case the first lens (f = 133 cm) has to be replaced by a lens of f = 63 cm.

The energy density was varied by changing the position of the target along the axis of the ruby laser beam.

The target consists of a 25 x 28 x 1 mm glass slide with vacuum evaporated metal layers on one side. The thickness of the metal film ranged between 0.2 µm and 1.5 µm.

The target is tilted by an angle of 17° relative to the axis of the ruby laser beam in the direction of the drift tube and can be moved by a manipulator from outside so that a number of spots can be ablated without breaking the vacuum. The size of the spots was nearly circular with a diameter of 1 mm.

The ablated material beam passes through a drift tube to be analysed by various methods:

- At a distance of 108 cm from the target the cloud passed an observation volume of 0.18 cm^3, where the atoms in the ground state were excited by a tunable flash lamp pumped dye laser in crossed beam geometry and were detected by laser-induced fluorescence (LIF) using a photomultiplier tube (RC 4840).
  For the LIF-measurements of the Li-atom density the wavelength of the dye laser bem was adjusted to λ = 6708 Å. For the corresponding measurements on Al a KDP crystal was used for frequency doubling and a UG5-filter to block out the visible light. The wavelength was adjusted to λ = 3082 Å. Calibration of the absolute densities was done by Rayleigh scattering in Argon. This technique is described in detail in /6/.

- At the end of the drift tube, 140 cm away from the target, a quadrupole mass spectrometer system (Balzers QMG 511) with electron bombardment ionizer was set up. The detector was a 14 stage Cu-Be electron multiplier. The signal from the multiplier was fed into a low capacitance preamplifier and then displayed on an oscilloscope.

The experimental set-up is shown in Fig. 1.

3. Results and Discussion:

Lithium has been strongly favoured as material for injection, as it has a low mass and therefore a high penetration velocity. Furthermore, the strong resonance transistion at $\lambda = 6708$ Å makes Li easily accessible for laser-induced fluorescence techniques.

In this experiment two types of targets were used:

1) A layer of simultaneously evaporated Li and Al with a total thickness of < 2000 Å
2) A three-layer sandwich-target (manufactured by LeBow Co. California, USA) with 0.5 µm Al, 0.5 µm Li and 0.5 Al, i.e. a total thickness of 1.5 µm. The Al-layer on top of the Li-layer should serve as a protection against contamination (e.g. by wet air).

Experiments with simultaneously evaporated Li/Al

Fig. 2 shows the density of Li $n_L(t)$ measured with LIF using a target with simultaneously evaporated Li and Al. The peak density was found to be 5×10^9 cm^3, the peak energy 3.24 eV. Comparison of the time of flight (~70 µsec) with the half width of the pulse (~20 µsec) shows that the distribution is non-thermal /8/. The low density of Li compared with the measurements on Li in /3/ is probably due to the lower amount of Li evaporated during the complicated process of simultaneous evaporation.

Experiments with the Li/Al-sandwich targets

3.1.1 Surface Analysis

Before installation in the vacuum chamber a surface analysis of these targets was carried out. The results of this surface analysis using secondary ion mass spectroscopy (SIMS) are shown in Figs. 3 and 4 /9/.

The depth profile shows that the Li-layer has completely diffused to the surface of the metal film. Due to this segregation process the original three-layer target has changed to a two-layer target with 0.5 µm Li covering 1 µm Al. The segregation process of binary metal systems is discussed in /10,11,12/. The surface composition of an alloy of Li and other metals changes with time due to segregation processes depending on the solution enthalpies, the surface energies, the different sizes of the atoms and the temperature. Using the model of Miedema /10/ it was calculated that in the case of an Li-Al-alloy this effect results in a complete segregation of Li and Al at a temperature of 300 K. The surface concentration of Li reaches a value of 100 % (cf. Fig. 5) /13/. A similar phenomenon can be observed with these three-layer-targets.

A second depth profile analysis (Fig. 4) shows the presence of six different materials on the same target. A part of the Al seems to be oxidized as Al_2O_3, another part is in the form of LiAl-molecules. Hydrogen and oxygen turned out to be the most abundant impurities in the layers. The similarity of the Li- and H-curves leads to the assumption that the Li was present in the form of LiOH-molecules, since Li has reacted with the water vapor in the air. It should be noted that the analysis is only qualitative but not quantitative.

One of the sandwich-targets was also analysed by optical microscopy. The microscopic views (dark-field illumination) showed a light-dark structure on the target, which can also be seen by the naked eye. To stretch the contrast, pictures were made with the light coming from one side only revealing the light-dark structures as surface features on the target. It can be seen that the thickness of the metal film changes depending on the position of the target. Small "craters" at the target surface are also present (Fig. 6), and in the target material a "bubble"-like structure can be seen (Fig. 7) (see also the pictures given in /14/). In air at normal pressure the light-dark structures on the target-surface become coloured. In the SIMS-vacuum chamber with a base pressure in the range of 10^{-10} mbar part of the metal film scaled off the glass slide.

3.1.2 Ablation measurements

The results of the LIF-measurements in the case of the sandwich target look quite different from those in the case of the target with simultaneously evaporated Li-Al coating concerning the energy distribution and the density (Fig. 8). The peak densities were found to be 1×10^{10} cm^{-3} for Al and 8×10^{10} cm^{-3} for Li. The energies at the density peaks turned out to be 15 eV for Al and 1 eV for Li. The half widths were found to be 50 µsec for Al and 200 µsec for Li. Compared with the time of flight the Li-beam shows a nearly thermal distribution, while the Al-beam is not thermal.

Fig. 9 shows a comparison of the density-distribution of Li with a Maxwellian of a temperature of 1.1 eV using a least square fit.

A comparison of the energy distribution of Al ablated with an energy density of 9.7 Jcm^{-2} and 6.0 Jcm^{-2}, respectively, shows that a slight reduction of the energy density causes only a smaller peak density while the peak energy remains roughly the same (Fig. 10). With an increase of the energy density to 30 Jcm^{-2} the peak energy of Al changes from 15 eV to 27 eV. This result was also found be Breton et al. /7/.

The increase of the energy density produces a second maximum in the density with a peak energy of 12 eV (Fig. 11). Similar results were reported in /3/ for Li.

The results are summarized in Table 1.

The results of the surface analysis described above can deliver a reasonable explanation for this behaviour. When the layer is heated by the ruby laser pulse and the temperature of the Al-layer reaches the boiling point of Li, the Li evaporates freely from the target, yielding a nearly thermal distribution. The Al-layer which is liquid at this temperature is then heated up to still higher temperatures so that the lower part of the layer is in the form of Al-vapour between the glass and the liquid surface of the layer. The Al is then ablated at much higher energies than the Li yielding a sharp non-thermal distribution. The ablation- (and evaporation-) processes take place in the range of tens of nanoseconds. Since the flight time from the target to the observation volume is several hundred microseconds the Al-cloud gets ahead of the Li-cloud reaching the observation volume $\sim$150 µs earlier than the latter one.

3.2 Comparison of the LIF-measurements with quadrupole mass spectroscopy

In addition to the LIF-measurements we also used quadrupole mass spectroscopy.

Fig. 12 shows a typical QMS-signal on mass 27. Earlier investigations showed that both neutral and ionized atoms are generated by laser irradiation with the ions being typically 3 times more energetic than the neutrals /5/. Due to these measurements Lie et al. supposed that the first peak represents the ionized atoms while the following peaks are due to the neutrals /3/.

According to our measurements the first peak of the QMS-signal seems to consist of neutral atoms while the following spikes are due to clusters of atoms as discussed in /4/. The time of flight and the amplitude of these spikes varied by a factor of 2-3 from shot to shot. An explanation for the generation of clusters may be the liquid state of the surface of the Al-layer at the time of ablation.

3.3 Optical microscopic analysis

After the ablation experiments the targets were analysed by optical microscopy. The structure of the spots was compared with the structure of spots of ablated pure Al-targets (thickness 3 µm).

The microscopic views show clearly the different ablation processes of a pure aluminium target (Fig. 13) and a target of Al combined with Li (Fig. 14).

In the case of the pure Al-targets all material within the area corresponding to the cross section of the ruby laser beam has been ablated leaving a nearly circular spot of 1 mm in diameter with a sharp defined edge.

In the case of the Li/Al-Targets ablated under the same conditions, the spots show a roughly circular center where the material is completely ablated but at the edges exfoliation leaves a structured region of about one spot-radius around the ablated center. In the case of lower energy densities, i.e. larger spot diameter, a part of the material in the center of the spot is left on the glass slide while an annular region is completely ablated. Ablation of the pure Al-target under this conditions leaves a larger spot, the area of which is still covered with a thin layer of material.

The microscopic views also show that a part of the ablated material has been redistributed on the target surface. Probably high field strength produced by the laser beam causes some of the ionized material to fall back onto the target. At a distance of some mm from the spots radial structures looking like ejected material around lunar craters can be seen.

Acknowledgements

The authors wish to thank Prof. E. Hintz for his encouragement and for valuable discussions during this work.

We also thank Mr. S. Musso and Mr. H. Priesent for assisting the experiment and Mr. H. Overkott for preparing some of the targets.

We would like to thank Mr. K.H. Besocke, Mrs. G. Flentje and Dr. K.G. Tschersich of the Institut für Grenzflächenforschung und Vakuumphysik for the surface analysis of the targets.

One of us (S.M.R.) would like to thank Prof. L. El-Nadi for the help to get the fellowship and acknowledges gratefully the support of the International Office of the KFA during his stay.

References

/1/ K. Kadota, A. Pospieszczyk, P. Bogen, E. Hintz
Jül Report 1812, Oct. 1982

/2/ K. Kadota, A. Pospieszczyk, P. Bogen, E. Hintz
IEEE Transactions on Plasma Science (1984), to be published

/3/ Y.T. Lie, A. Pospieszczyk, J.A. Tagle
Nuclear Technology/Fusion (1984), to be published

/4/ D. Manos, D. Ruzic, R. Moore, S. Cohen
J. Vac. Sci. Technol. 20, (1982), 1230-1233

/5/ E.S. Marmar, J.L. Cecchi, S.A. Cohen
Rev. Sci. Instrum. 46, (1975), 1149-1154

/6/ P. Bogen, Y.T. Lie,
J. Nucl. Mat. 93 & 94 (1980) 363-367

/7/ C. Breton, C. de Michelis, W. Hecq, M. Mattioli
Revue Phys. Appl. 15 (1980), 1193-1200

/8/ A. Pospieszczyk, P. Bogen, H. Hartwig, Y.T. Lie
J. Nucl. Mat. 93 & 94 (1980), 368 - 371

/9/ K.H. Besocke, G. Flentje, K.G. Tschersich,
private communication

/10/ A.R. Miedema, Z. Metallkde
69 (1978), 455-461

/11/ D.M. Gruen, A.R. Krauss, S. Susman, M. Venugopalan,
M. Ron J. Vac. Sci. Technol. A1 (1983), 924-928

/12/ A.R. Krauss, D.M. Gruen, A.BA. Dewald,
J. Nucl. Mat. 121, (1984) 398-403

/13/ R.P. Schorn, private communication

/14/ S.P. Yatsenko, K.A. Chuntonov, S.I. Alyamovskij, E.N. Dieva
(1971)
Zakonomernosti stroeniya diagramm sostoyaniya
shchelochnykl metallov s metallami III b gruppy

Figure Captions

Fig. 1 Experimental set up

Fig. 2 Density distribution of Li generated by laser ablation of a Li-Al-film obtained by simultaneous evaporation of the metals.

Fig. 3 Depth profile of Li and Al in the three-layer Al/Li/Al-target measured by SIMS.

Fig. 4 Depth profile of Li, Al, LiAl, AlO, H and O in the three-layer Al/Li/Al-target measured by SIMS.

Fig. 5 Calculation of the Li-concentration at the surface of a Li-Al-alloy as a function of the bulk concentration and the temperature of the probe.

Fig. 6 Microscopic view of the surface features of the Al/Li/Al-target (illumination from the top)

Fig. 7 Microscopic view of the surface of the Al/Li/Al-target (dark-field illumination)

Fig. 8 Comparison of the density distributions of Al and Li, ablated from a sandwich-target.

Fig. 9 Comparison of the energy distribution of Li with a Maxwellian corresponding to a temperature of 1.1 eV.

Fig. 10 Comparison of the distribution of Al ablated with different energy densities of the ruby laser beam at the target.

Fig. 11 Density distribution of Al ablated with an energy density of $30\ Jcm^{-2}$.

Fig. 12 QMS-signal on mass 27 (Aluminum).

Fig. 13 Microscopic view of a spot ablated from pure Al-target (thickness 3 µm).

Fig. 14 Microscopic view of a spot ablated from a Li/Al target (Li 500 Å, Al 800 Å).

Target	Element observed	Energy density Jcm^{-2}	Time of flight µs	Peak velocity $\times 10^{5}$ cms^{-1}	Peak energy eV	Peak density $\times 10^{10}$ cm^{3}
Li/Al 2000 Å	Li	7.6	67	16	3.24	0.5
Al/Li/Al 5000 Å each Target 1	Li	6.9	250	4.8	0.68	8.0
	Al	9.7	105	10.3	14.8	0.9
		6.0	105	10.3	14.3	0.6
Al/Li/Al 5000 Å each Target 2	Al	29.9	77.5	13.9	26.98	1.4
	(second Maximum)		(118)	(9.2)	(11.7)	(0.6)

Table 1

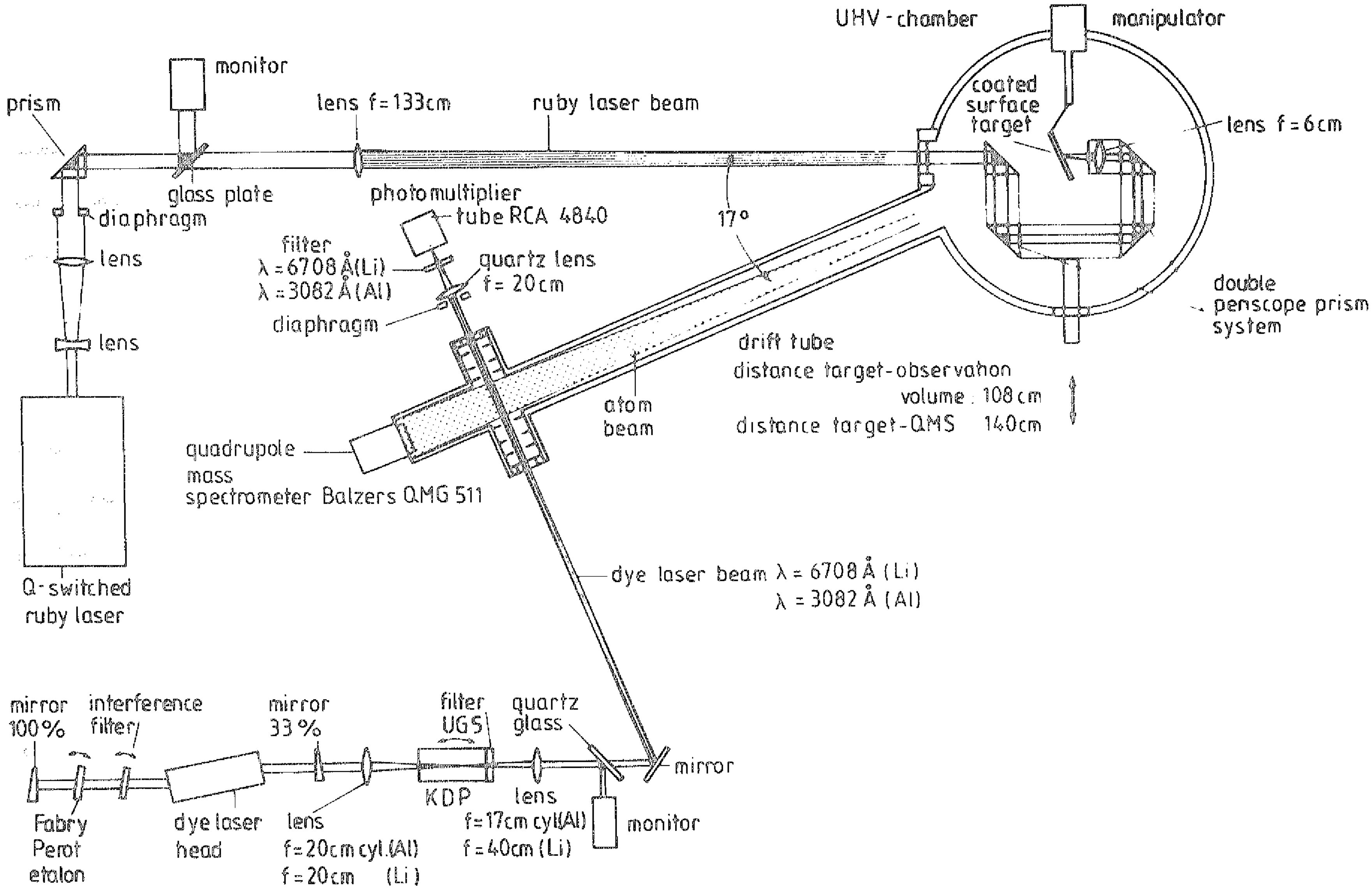

Fig. 1 Experimental set up

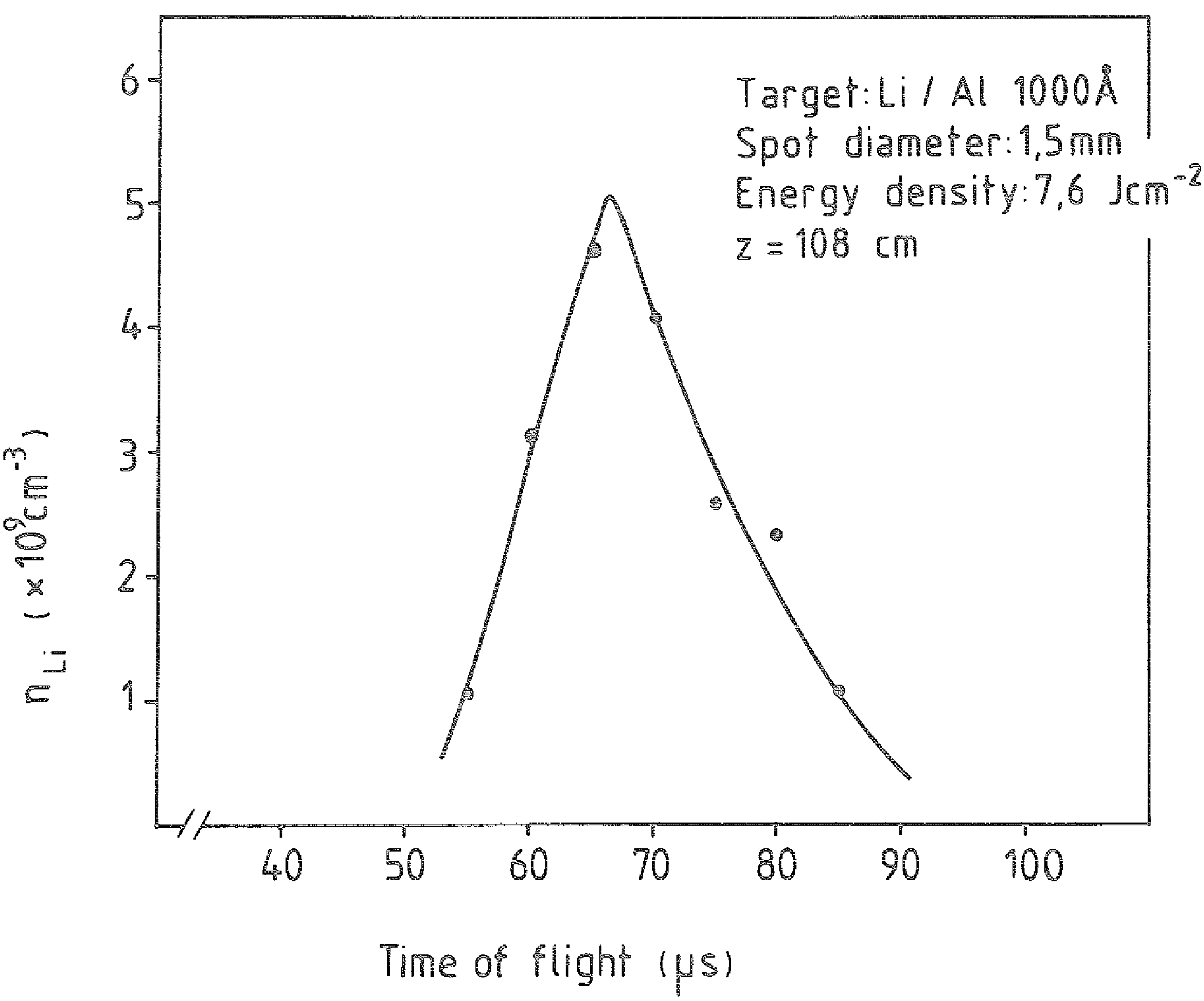

Fig. 2 Density distribution of Li generated by laser ablation of a Li-Al-film obtained by simultaneous evaporation of the metals.

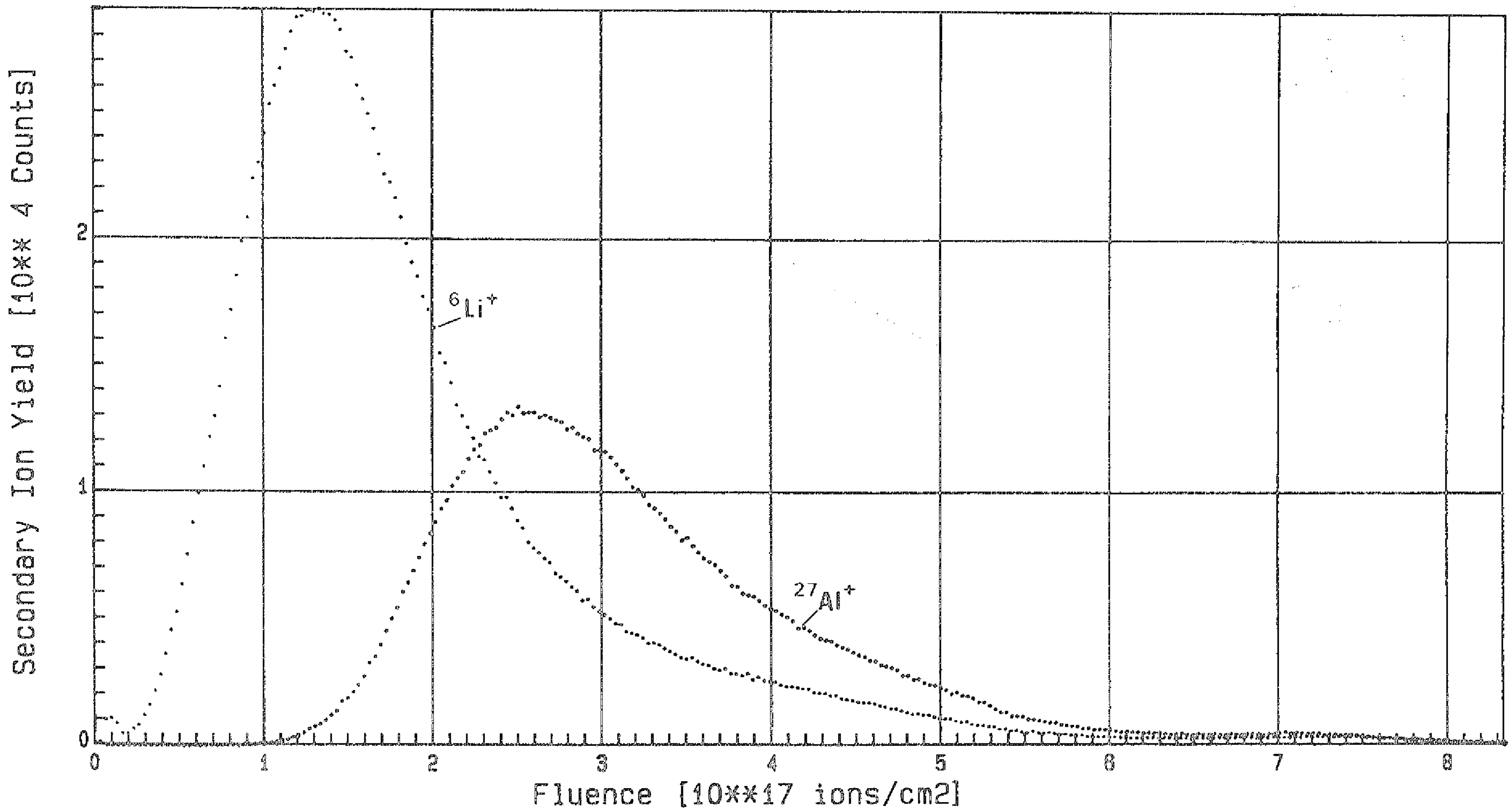

Fig. 3 Depth profile of Li and Al in the three-layer Al/Li/Al-target measured by SIMS.

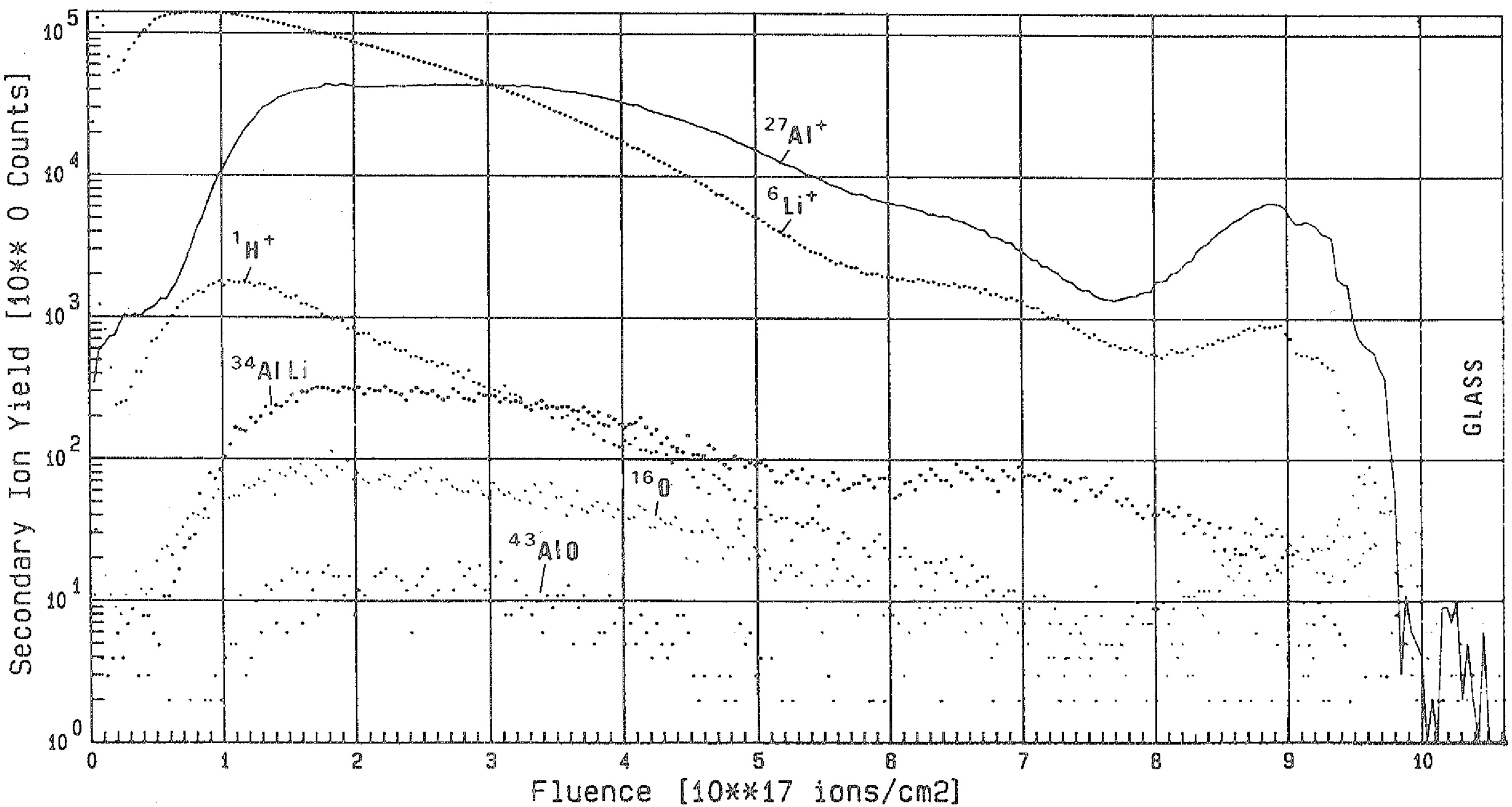

Fig. 4 Depth profile of Li, Al, LiAl, AlO, H and O in the three-layer Al/Li/Al-target measured by SIMS.

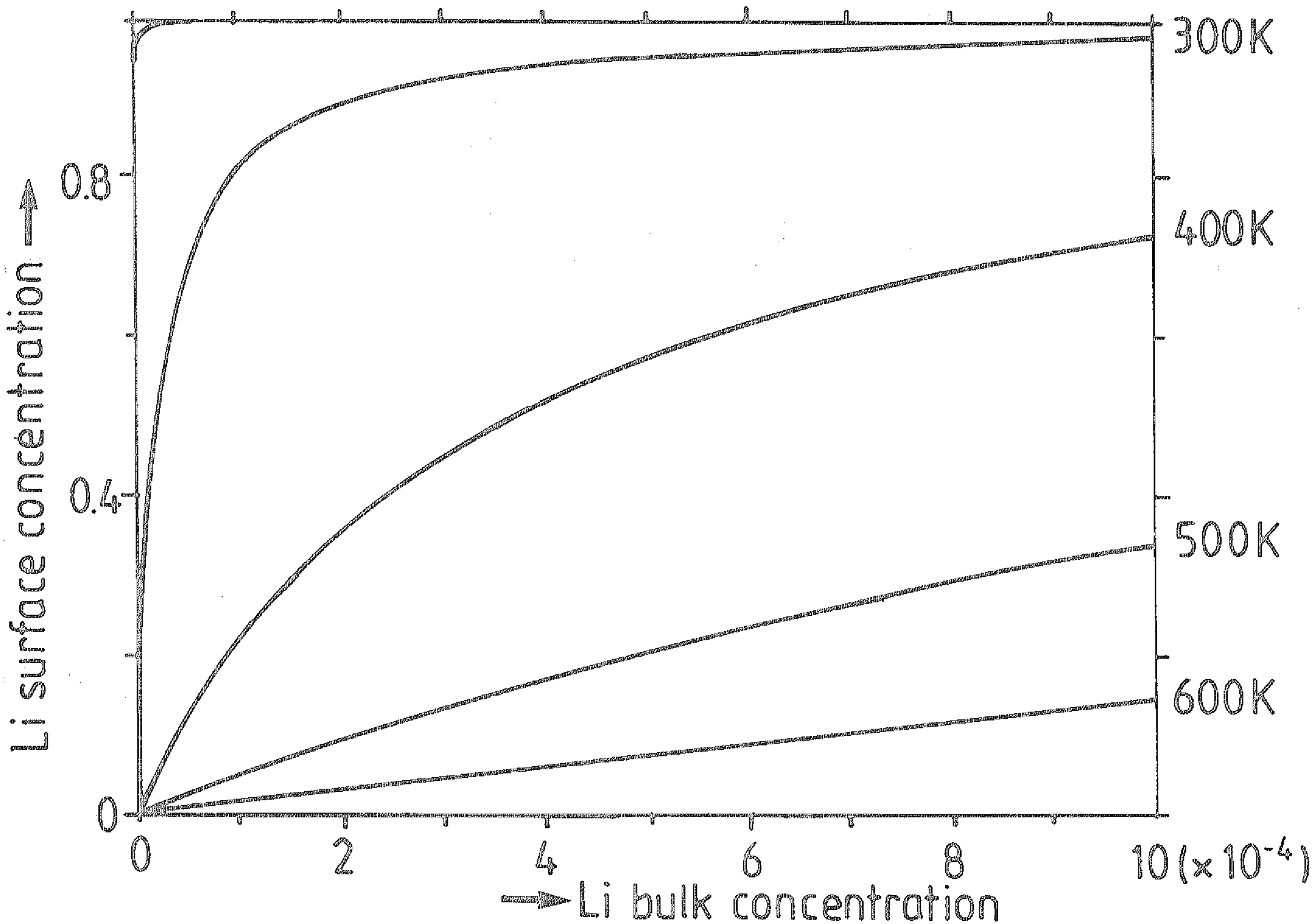

Fig. 5 Calculation of the Li-concentration at the surface of a Li-Al-alloy as a function of the bulk concentration and the temperature of the probe.

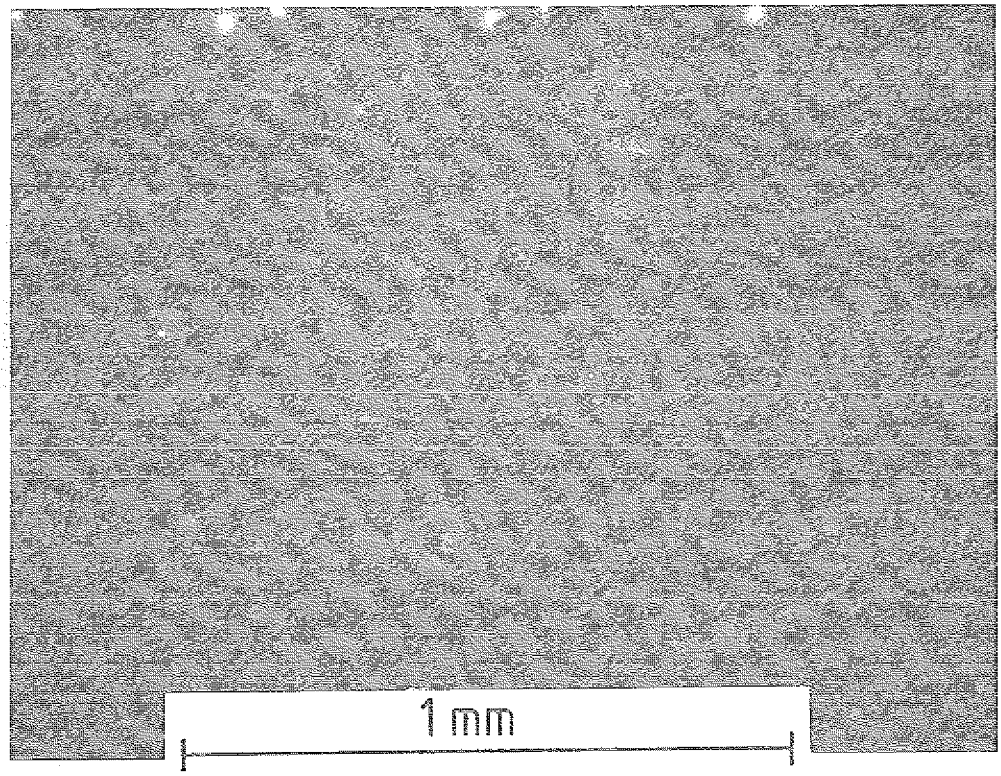

Fig. 6 Microscopic view of the surface features of the Al/Li/Al-target (illumination from the top)

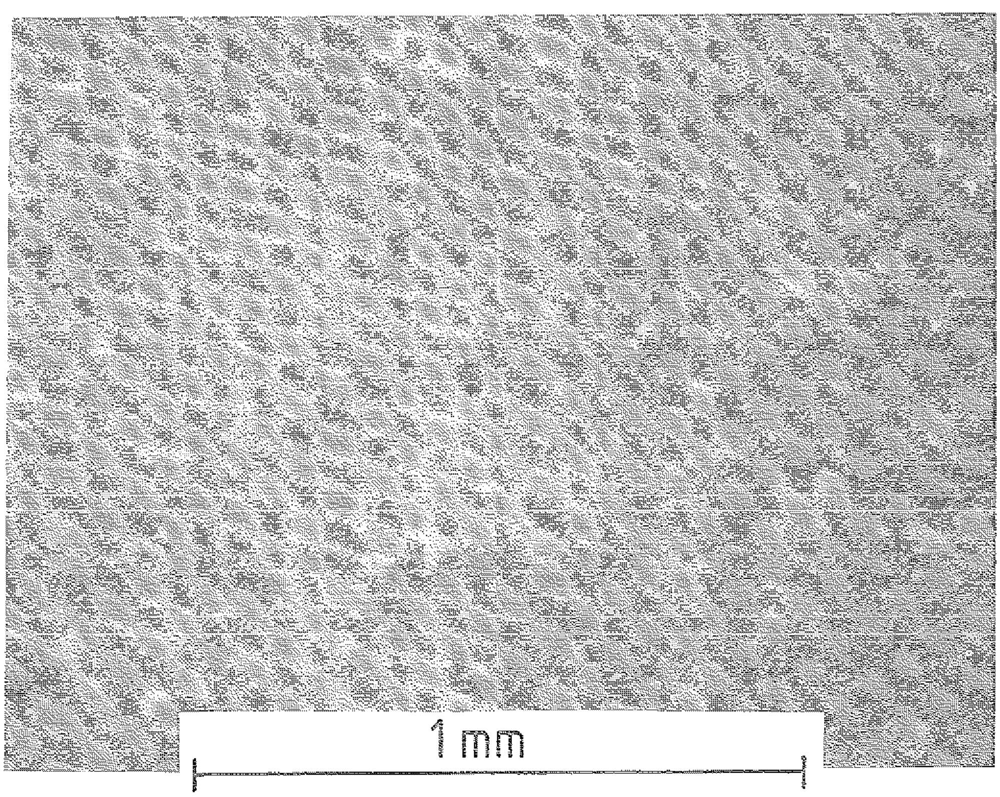

Fig. 7 Microscopic view of the surface of the Al/Li/Al-target (dark-field illumination)

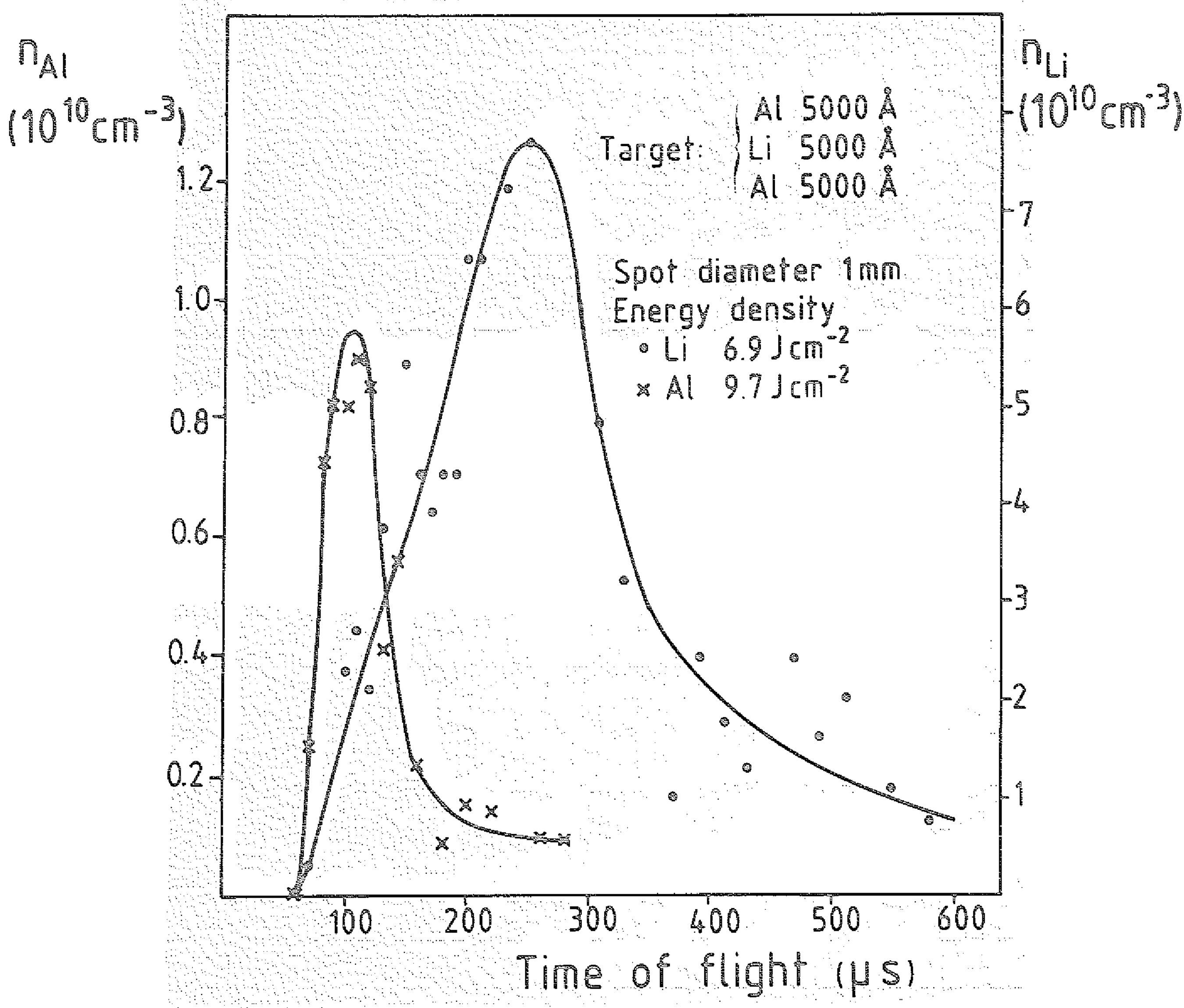

Fig. 8 Comparison of the density distributions of Al and Li, ablated from a sandwich-target.

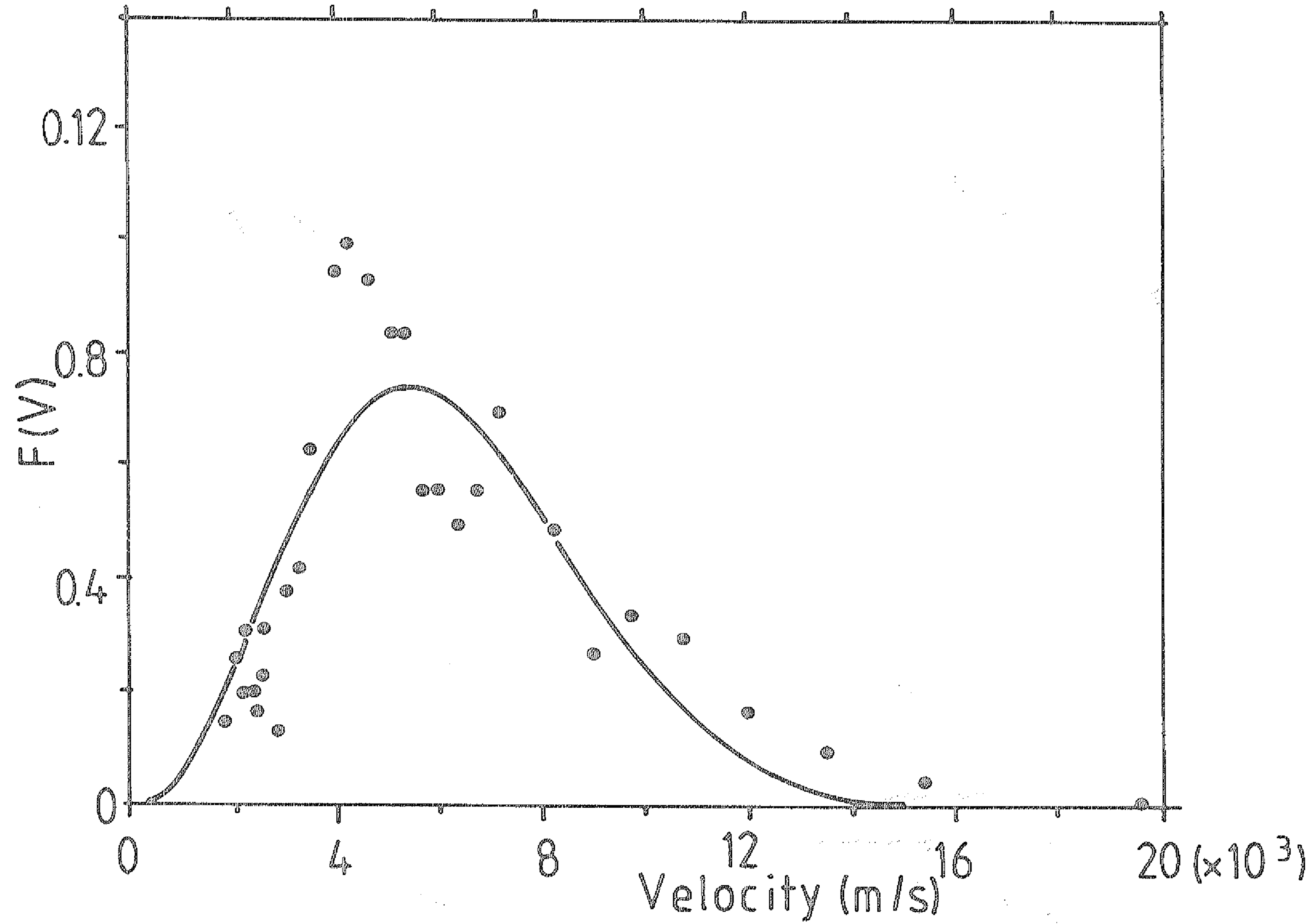

Fig. 9 Comparison of the energy distribution of Li with a Maxwellian corresponding to a temperature of 1.1 eV.

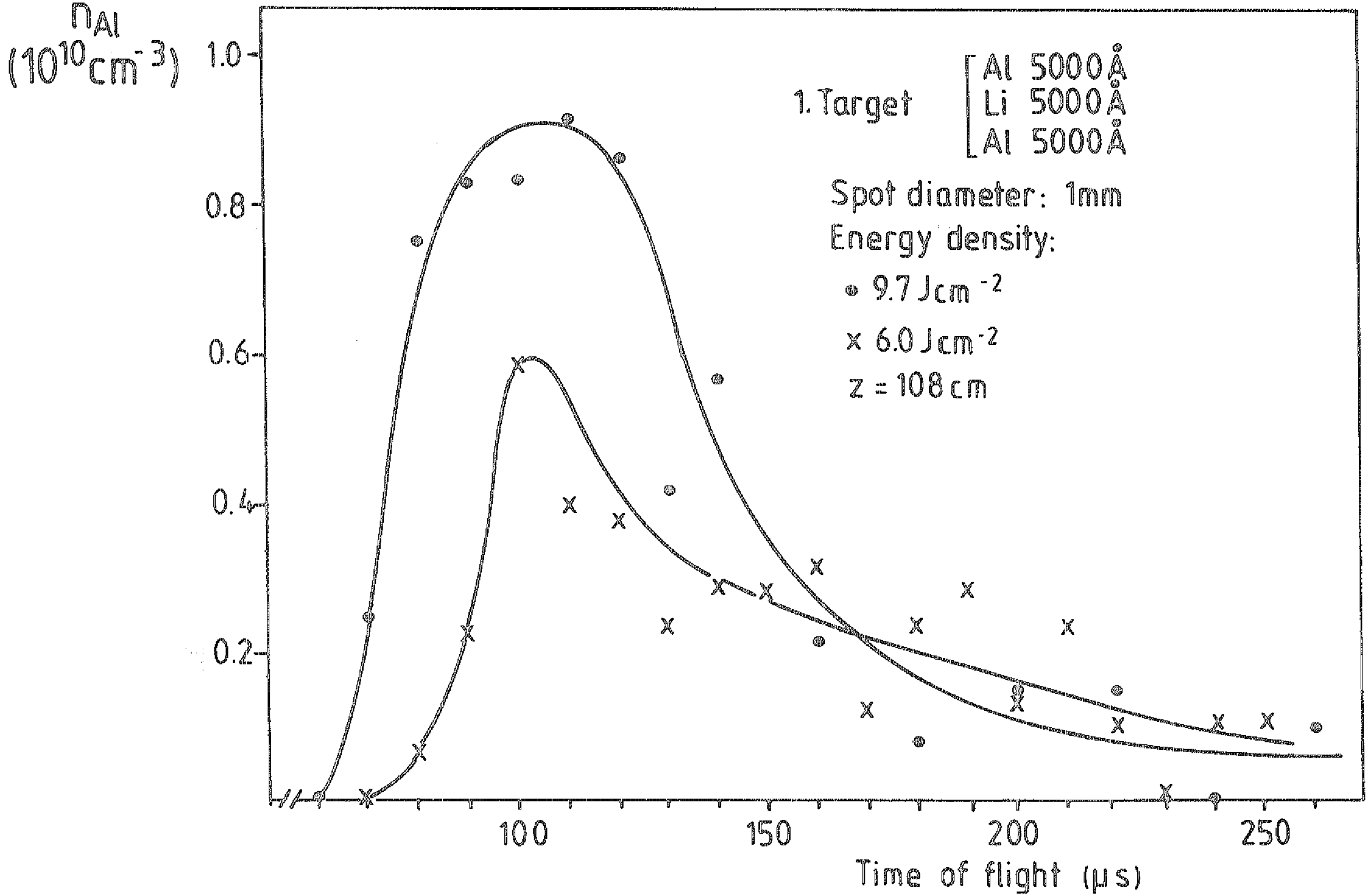

Fig. 10 Comparison of the distribution of Al ablated with different energy densities of the ruby laser beam at the target.

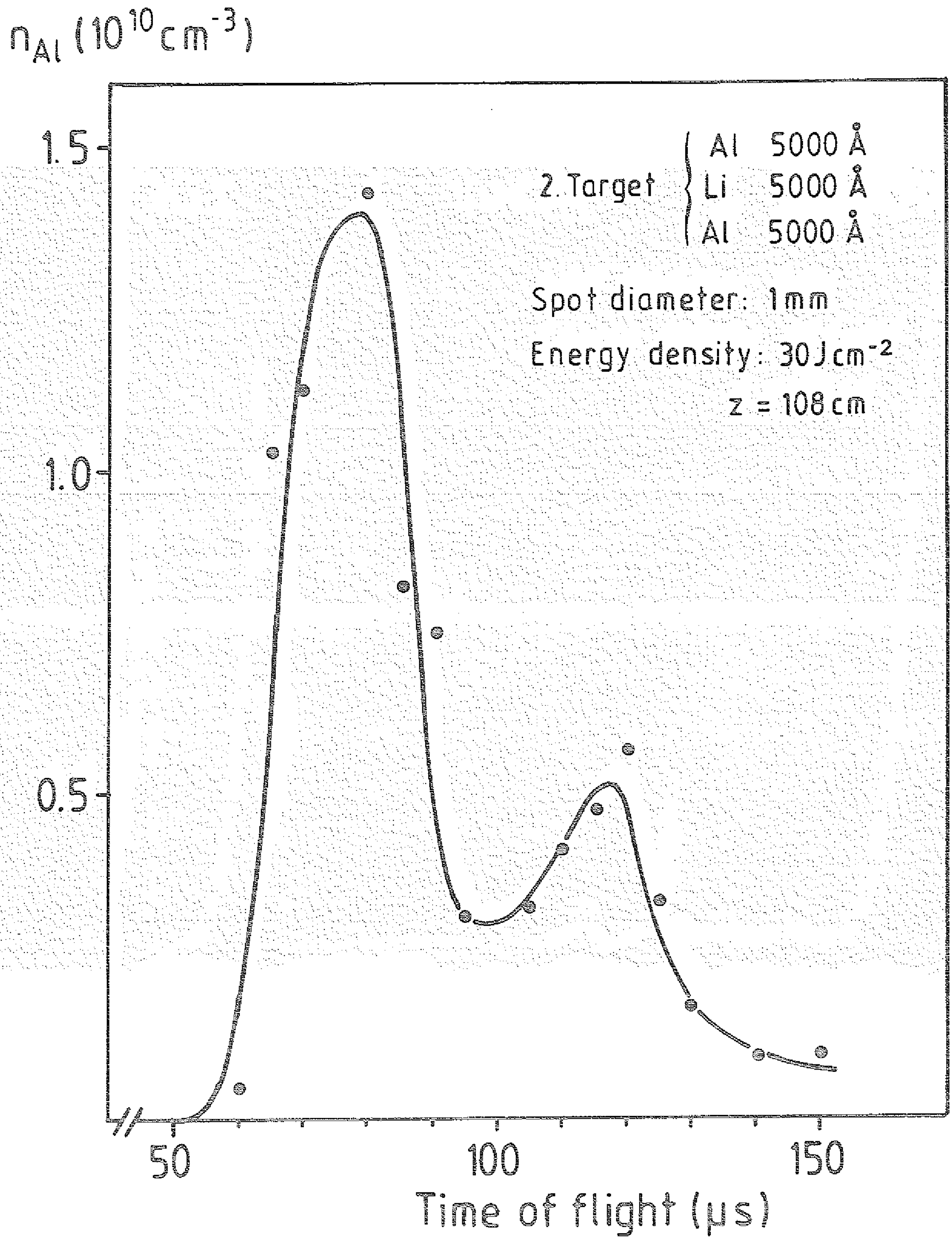

Fig. 11 Density distribution of Al ablated with an energy density of 30 Jcm^{-2}.

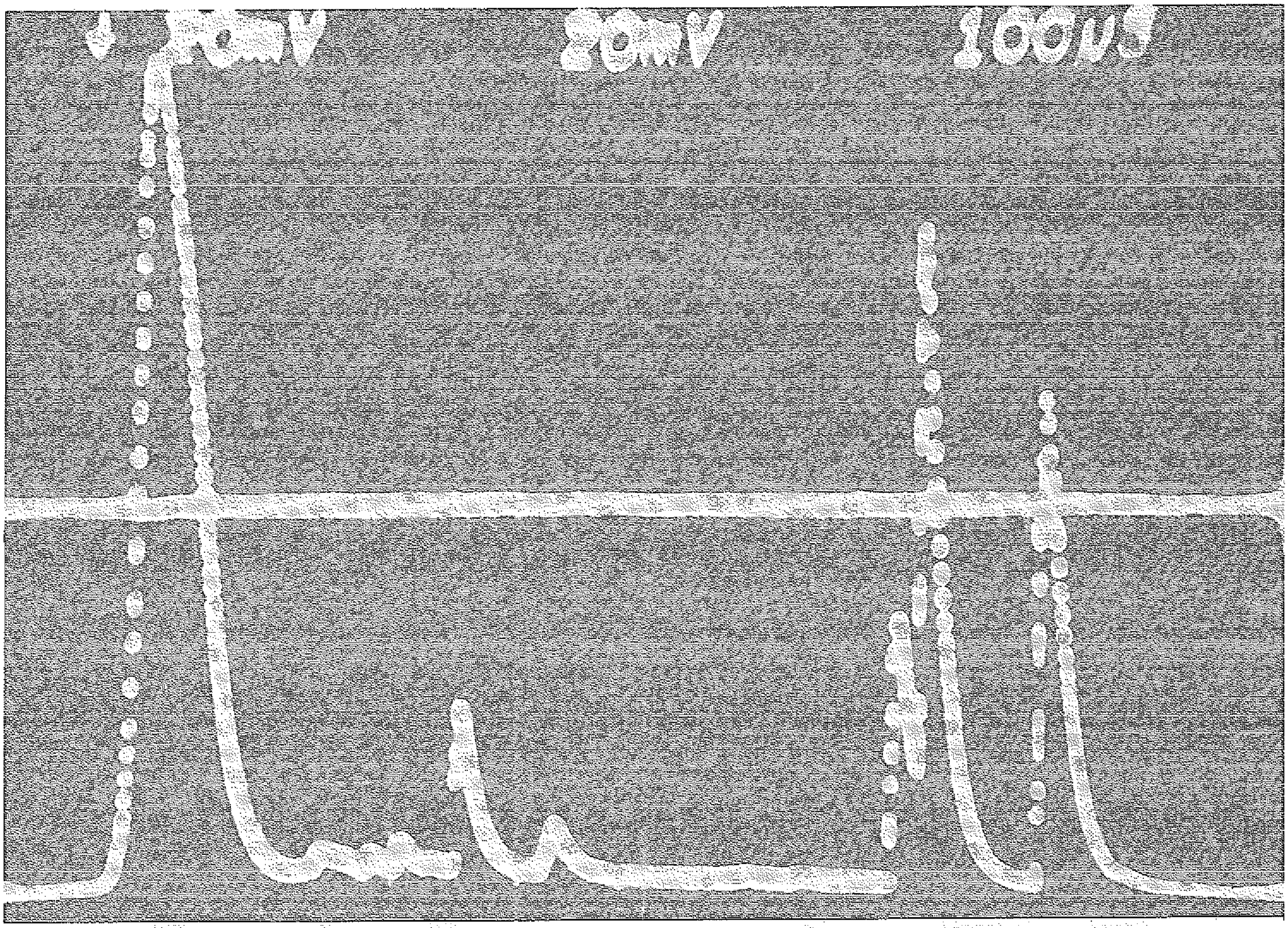

Fig. 12 QMS-signal on mass 27 (Aluminum).

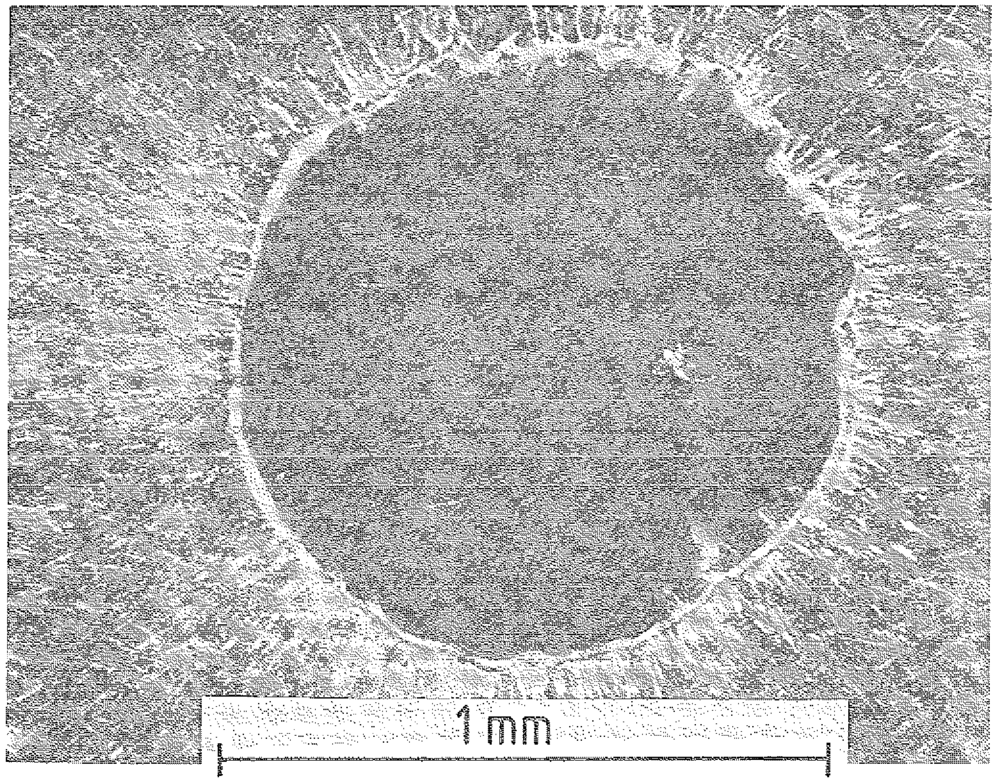

Fig. 13 Microscopic view of a spot ablated from pure Al-target (thickness 3 µm).

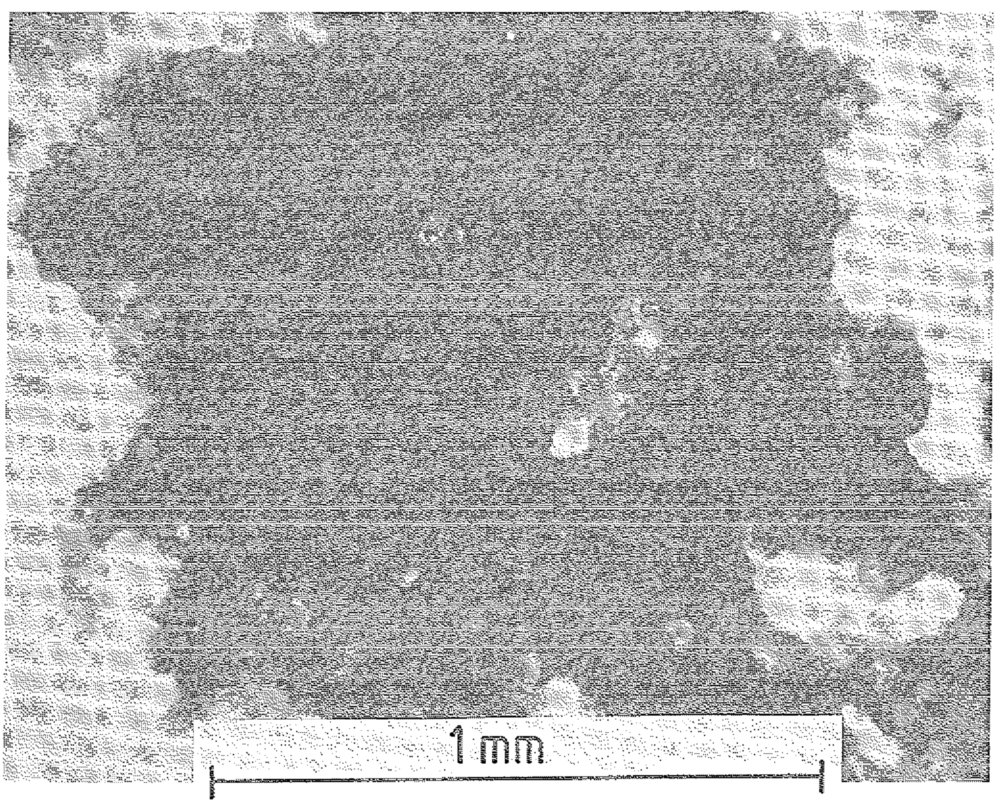

Fig. 14 Microscopic view of a spot ablated from a Li/Al target (Li 500 Å, Al 800 Å).